Inorg. Chem. **2007**, *46*, 6437–6443

From Pseudo to True C_3 Symmetry: Magnetic Anisotropy Enhanced by Site-Specific Ligand Substitution in Two Mn_{15}-Carboxylate Clusters

Yan-Zhen Zheng, Wei Xue, Wei-Xiong Zhang, Ming-Liang Tong,* and Xiao-Ming Chen*

MOE Laboratory of Bioinorganic and Synthetic Chemistry/State Key Laboratory of Optoelectronic Materials and Technologies, School of Chemistry & Chemical Engineering, Sun Yat-Sen University, Guangzhou 510275, China

Received March 8, 2007

Two new mixed-valence manganese–carboxylate clusters, $[Mn^{III}_9Mn^{IV}_6(O_2CPh)_{12}(\mu_3\text{-}O)_{13}(\mu\text{-}O)_4(\mu\text{-}OMe)_5(MeOH)_4(H_2O)_5]_2\cdot 1.5PhCO_2H\cdot MeOH\cdot 6H_2O$ (**1**, $PhCO_2H$ = benzoic acid) and $[Mn^{III}_9Mn^{IV}_6(O_2CCh)_{12}(\mu_3\text{-}O)_{13}(\mu\text{-}O)_4(\mu\text{-}OMe)_5(MeOH)_3(H_2O)_6]\cdot 0.5MeOH\cdot 2.5H_2O$ (**2**, $ChCO_2H$= cyclohexanecarboxylic acid) contain new disklike Mn_{15} cores. Both **1** and **2** can be synthesized by the conventional manganese redox reaction (MnO_4^- oxidizing Mn^{2+}) in methanol solution. **2** can be also synthesized via the site-specific ligand substitution reaction from **1**. **1** crystallizes in the triclinic space group $P\bar{1}$, whereas **2** crystallizes in the trigonal space group $P\bar{3}$. Magnetic study shows that both **1** and **2** have the same ground spin states $S_T = 2$. Compared to the silence of the out-of-phase ac susceptibility of **1**, **2** shows clearly slow magnetic relaxation behavior above 1.8 K due to the dramatically enhanced axial magnetic anisotropy ($D = -0.89$ and -1.58 cm^{-1} for **1** and **2**, respectively, which was obtained by fitting the plots of M vs H/T with the program ANISOFIT 2.0).

1. Introduction

The research for single-molecule magnets (SMMs) with a higher blocking temperature has accelerated the synthetic efforts aimed at the structural control of cluster architecture with large ground-spin states (S_T) and axial zero-field splitting parameters (D_m).[1] The increase of S_T is obviously based on ferromagnetic interactions between the spins,[1,2] whereas the enhancement of the D_m is mainly associated with the magnetic anisotropy of the cluster, which in turn depends on the local anisotropies of the single ions and their vectorial addition to give a resulting anisotropy.[1,2] Because the D_m tensor is mainly determined by the projection of a single-site zero-field-splitting parameter (D_i) onto S_T, D_m may vanish when the metal−ion arrangement approaches a cubic symmetry.[2] Moreover, quantum tunneling magnetization (QTM) is related to the second-order transverse magnetic anisotropy (E_m), which is exactly zero for molecules with strictly axial symmetry.[3] Thus, the control of molecular topology is critical in tuning molecules with large energy barriers and controlling QTM mechanisms.

After understanding the origin of magnetic anisotropy, a lot of synthetic effort has been paid to prepare or modify molecules in a controlled fashion.[4] An elegant strategy is based on the site-specific modification of preformed cluster architectures, which was first introduced in studying the chemical environments on the magnetic properties of the famous Mn_{12} clusters by substituting a variety of outer-

* To whom correspondence should be addressed. E-mail: tongml@mail.sysu.edu.cn (M.-L.T.), cxm@mail.sysu.edu.cn (X.-M.C.). Fax: (+)-86 20 8411-2245.

(1) For reviews, see (a) Christou, G.; Gatteschi, D.; Hendrickson, D. N.; Sessoli, R. *MRS Bull.* **2000**, *25*, 66−71. (b) Gatteschi, D.; Sessoli, R. *Angew. Chem., Int. Ed.* **2003**, *43*, 268−297. (c) Aromí, G.; Brechin, E. K. *Struct. Bonding* **2006**, *122*, 1−67.

(2) (a) Gatteschi, D.; Sorace, L. *J. Solid State Chem.* **2001**, *159*, 253−261. (b) Oshio, H.; Nakano, M. *Chem.—Eur. J.* **2005**, *11*, 5178−5185. (c) Bencini, A.; Gatteschi, D. *EPR of Exchange Coupled Systems*; Springer-Verlag: Berlin, Germany, 1990.

(3) (a) Chudnosky, E. M.; Tejada, J. *Macroscopic Quantum Tunneling of the Magnetic Moments*; Cambridge University Press: Cambridge, U.K., 1998. (b) Gunther, L.; Barbara, B. *Quantum Tunneling of the Magnetization-QTM '94*; Kluwer: Dordrecht, The Netherlands, 1995.

(4) (a) Andres, H.; Basler, R.; Güdel, H.-U.; Aromí, G.; Christou, G.; Büttner, H.; Rufflé, B. *J. Am. Chem. Soc.* **2000**, *122*, 12469−12477. (b) Oshio, H.; Hoshino, N.; Ito, T.; Nakano, M. *J. Am. Chem. Soc.* **2004**, *126*, 8805−8812. (c) Zaleski, C. M.; Depperman, E. C.; Dendrinou-Samara, C.; Alexiou, M.; Kampf, J. W.; Kessissoglou, D. P.; Kirk, M. L.; Pecoraro, V. L. *J. Am. Chem. Soc.* **2005**, *127*, 12862−12872. (d) Accorsi, S.; Barra, A.-L.; Caneschi, A.; Chastanet, G.; Cornia, A.; Fabretti, A. C.; Gatteschi, D.; Mortalo, C.; Olivieri, E.; Parenti, F.; Rosa, P.; Sessoli, R.; Sorace, L.; Wernsdorfer, W.; Zobbi, L. *J. Am. Chem. Soc.* **2006**, *128*, 4742−4755. (e) Ribas-Arino, J.; Baruah, T.; Pederson, M. R. *J. Am. Chem. Soc.* **2006**, *128*, 9497−9505. (f) Glaser, T.; Heidemeier, M.; Weyhermüller, T.; Hoffmann, R.-D.; Rupp, H.; Müller, P. *Angew. Chem., Int. Ed.* **2006**, *45*, 6033−6037.

10.1021/ic7004584 CCC: $37.00
Published on Web 07/13/2007

coordinated carboxylates, although showing only small perturbations on the magnetic anisotropy.[5] This strategy represents a leap in using organically soluble species of SMMs for further surface modification[6] or as subsecondary building units in molecular assembly.[7] An exciting result among the current limited examples derived by this strategy was recently observed in a Fe_4 SMM, in which the symmetry of the Fe_4 clusters was raised from C_2 to D_3 with 2-fold enhancement of the D_m value or magnetic anisotropy,[8] thus implying a promising way to enhance the magnetic anisotropy of the current SMMs.

High nuclearity manganese cluster complexes provide a fertile source for new SMMs. The known manganese cluster sizes greater than 12 include Mn_{13}, Mn_{16}, Mn_{18}, Mn_{19}, Mn_{21}, Mn_{22}, Mn_{25}, Mn_{26}, Mn_{30}, Mn_{32}, and Mn_{84}.[9] However, these species usually do not exhibit the ligand substitution reaction, possibly because of the insolubility or instability of the large clusters. Herein, we present another site-specific ligand substitution reaction that first takes place on a manganese cluster with a size greater than 12, namely $[Mn^{III}_9Mn^{IV}_6(O_2CPh)_{12}(\mu_3\text{-}O)_{13}(\mu\text{-}O)_4(\mu\text{-}OMe)_5(MeOH)_4(H_2O)_5]_2\cdot 1.5PhCO_2H\cdot MeOH\cdot 6H_2O$ (**1**, $PhCO_2H$ = benzoic acid), in which the benzoate can be substituted by cyclohexanecarboxylate to furnish $[Mn^{III}_9Mn^{IV}_6(O_2CCh)_{12}(\mu_3\text{-}O)_{13}(\mu\text{-}O)_4(\mu\text{-}OMe)_5(MeOH)_3(H_2O)_6]\cdot 0.5MeOH\cdot 2.5H_2O$ (**2**, $ChCO_2H$= cyclohexanecarboxylic acid). Moreover, this reaction leads to not only the symmetry of the Mn_{15} clusters enhanced from C_1 to C_3 but also the intermolecular interaction minimized from significant $\pi-\pi$ stacking to the pure van der Waals, in **1** and **2**, respectively, which results in the significant enhancement of the energy barrier for spin reversal in **2**.

2. Experimental Section

General Remarks. All of the chemicals were commercially available and used as received without further purification. The C, H, and N microanalyses were carried out with an Elementar Vario-EL CHNS elemental analyzer. FTIR spectra were recorded from KBr pellets in the range 4000−400 cm^{-1} on a Bio-Rad FTS-7 spectrometer.

Synthesis. Preparation of 1. To a methanol solution (30 mL) of benzoic acid (0.61 g, 5 mmol), $MnCl_2\cdot 4H_2O$ (0.198 g 1.0 mmol) and $KMnO_4$ (0.079 g 0.5 mmol) were added with magnetic stirring. The solution then turned black, and the beaker was sealed with a Parafilm for a further ca. 24 h of stirring. After filtration, the filtrate was allowed to stand at room temperature. After two weeks, black platelike crystals of **1** were collected and washed with acetone (30−40% yield based on Mn). IR data for **1** (KBr, cm^{-1}): 3380 m, 1703 m, 1596 vs, 1558 s, 1510 s, 713 s, 670 s, 648 s, 613 s, 551 m, 522 m. Anal. Calcd for **1**: C, 38.45; H, 3.71; Found: C, 38.49; H, 3.65.

Preparation of 2. 2 can be prepared in a similar way to **1** except that cyclohexanecarboxylic acid was used instead of benzoic acid. **2** can be also prepared from **1**, that is **1** (0.308 g, 0.05 mmol) was dissolved in $MeOH/Et_2O$ (1:4 v/v, 40 mL) and treated with cyclohexanecarboxylic acid (0.128 g, 1.0 mmol). After 12 h of stirring, the black solution becomes homogeneous. Black prismatic crystals of **2** were obtained after one week (60−70% yield based on Mn). IR data for **2** (KBr, cm^{-1}): 3425 m, 2955 m, 2853 m, 1601 vs, 1548 s, 1444 s, 1410 s, 1040 m, 930 m, 856 m, 763 w,-700 m, 612 m, 525 m, 448 w. Anal. Calcd for **2**: C, 36.52; H, 5.90; Found: C, 36.59; H, 5.82.

X-ray Study. Diffraction intensities of **1** and **2** were collected on a Bruker Apex CCD area-detector diffractometer (Mo Kα, λ = 0.71073 Å). Absorption corrections were applied by using multiscan program SADABS.[10] The structures were solved with direct methods and refined with a full-matrix least-squares technique with the SHELXTL program package.[11] Anisotropic thermal parameters were assigned to all non-hydrogen atoms. The organic hydrogen atoms were generated geometrically (C−H 0.96 Å) as well as the aqua hydrogen atoms (O−H 0.85 Å). Data collection parameters

(5) (a) Artus, P.; Boskovic, C.; Yoo, J.; Streib, W. E.; Brunel, L.-C.; Hendrickson, D. N.; Christou, G. *Inorg. Chem.* **2001**, *40*, 4199−4210. (b) Boskovic, C.; Pink, M.; Huffman, J. C.; Hendrickson, D. N.; Christou, G. *J. Am. Chem. Soc.* **2001**, *123*, 9914−9915. (c) Soler, M.; Artus, P.; Folting, K.; Huffman, J. C.; Hendrickson, D. N.; Christou, G. *Inorg. Chem.* **2001**, *40*, 4902−4912. (d) Pacchioni, M.; Cornia, A.; Fabretti, A. C.; Zobbi, L.; Bonacchi, D.; Caneschi, A.; Chastanet, G.; Gatteschi, D.; Sessoli, R. *Chem. Commun*. **2004**, 2604−2605. (e) Kuroda-Sowa, T.; Fukuda, S.; Miyoshi, S.; Maekawa, M.; Munakata, M.; Miyasaka, H.; Yamashita, M. *Chem. Lett.* **2002**, 682−683. (f) Bian, G.-Q.; Kuroda-Sowa, T.; Konaka, H.; Hatano, M.; Maekawa, M.; Munakata, M.; Miyasaka, H.; Yamashita, M. *Inorg. Chem.* **2004**, *40*, 4790−4792.

(6) (a) Cornia, A.; Costantino, A. F.; Zobbi, L.; Caneschi, A.; Gatteschi, D.; Mannini, M.; Sessoli, R. *Struct. Bonding* **2006**, *122*, 133−161. (b) Mannini, M.; Bonacchi, D.; Zobbi, L.; Piras, F. M.; Speets, E. A.; Caneschi, A.; Cornia, A.; Magnani, A.; Ravoo, B. J.; Reinhoudt, D. N.; Sessoli, R.; Gatteschi, D. *Nano Lett.* **2005**, *5*, 1435−1438. (c) Cavallini, M.; Biscarini, F.; Gomez-Segura, J.; Ruiz, D.; Veciana, J. *Nano Lett.* **2003**, *11*, 1527−1530. (d) Cornia, A.; Fabretti, A. C.; Pacchioni, M.; Zobbi, L.; Bonacchi, D.; Caneschi, A.; Gatteschi, D.; Biagi, R.; del Pennino, U.; de Renzi, V.; Gurevich, L.; van der Zant, H. S. J. *Angew. Chem., Int. Ed.* **2003**, *42*, 1645−1648. (e) Martínez, R. V.; García, F.; García, R.; Coronado, E.; Forment-Aliaga, A.; Romero, F. M.; Tatay, S. *Adv. Mater.* **2007**, *19*, 291−295.

(7) (a) Miyasaka, H.; Yamashita, M. *Dalton Trans.* **2007**, 399−406; and references therein. (b) Coulon, C.; Miyasaka, H.; Clérac, R. *Struct. Bonding* **2006**, *122*, 163−206; and references therein.

(8) Cornia, A.; Fabretti, A. C.; Garrisi, P.; Mortalò, C.; Bonacchi, D.; Gatteschi, D.; Sessoli, R.; Sorace, L.; Wernsdorfer, W.; Barra, A.-L. *Angew. Chem., Int. Ed.* **2004**, *43*, 1136−1139.

(9) For nuclearity larger than Mn_{12} clusters, see for examples: Mn_{13}, (a) Shanmugam, M.; Chastanet, G.; Mallah, T.; Sessoli, R.; Teat, S. J.; Timco, G. A.; Winpenny, R. E. P. *Chem.—Eur. J.* **2006**, *12*, 8777−8785. (b) Ferguson, A.; Thomson, K.; Parkin, A.; Cooper, P.; Milios, C. J.; Brechin, E. K.; Murrie, M. *Dalton Trans.* **2007**, 728−730; Mn_{16}, (c) Price, J. P.; Batten, S. R.; Moubaraki, B.; Murray, K. S. *Chem. Commun.* **2002**, 762−763. (d) King, P.; Wernsdorfer, W.; Abboud, K. A.; Christou, G. *Inorg. Chem.* **2004**, *43*, 7315−7323; Mn_{18}, (e) Brechin, E. K.; Sanudo, E. C.; Wernsdorfer, W.; Boskovic, C.; Yoo, J.; Hendrickson, D. N.; Yamaguchi, A.; Ishimoto, H.; Concolino, T. E.; Rheingold, X. A. L.; Christou, G. *Inorg. Chem.* **2005**, *44*, 502−511; Mn_{19}, (f) Ako, A. M.; Hwewitt, I. J.; Mereacre, V.; Clérac, R.; Wernsdorfer, W.; Anson, C. E.; Powell, A. K. *Angew. Chem., Int. Ed.* **2006**, *45*, 4926−4929; Mn_{21}, (g) Brockman, J. T.; Huffman, J. C.; Christou, G. *Angew. Chem., Int. Ed.* **2002**, *41*, 2506−2508; Mn_{22}, (h) Murugesu, M.; Raftery, J.; Wernsdorfer, W.; Christou, G.; Brechin, E. K. *Inorg. Chem.* **2004**, *43*, 4203−4209; Mn_{25}, (i) Murugesu, M.; Habrych, M.; Wernsdorfer, W.; Abboud, K. A.; Christou, G. *J. Am. Chem. Soc.* **2004**, *126*, 4766−4767. (j) Stamatatos, T. C.; Abboud, K. A.; Wernsdorfer, W.; Christou, G. *Angew. Chem., Int. Ed.* **2007**, *46*, 884−888; Mn_{26}, (k) Jones, L. F.; Brechin, E.; Collison, K.; Harrison, D. A.; Teat, S. J.; Wernsdorfer, W. *Chem. Commun*. **2002**, 2974−2975; Mn_{30}, (l) Soler, M.; Wernsdorfer, W.; Folting, K.; Pink, M.; Christou, G. *J. Am. Chem. Soc.* **2004**, *126*, 2156−2165; Mn_{32}, (m) Scott, R. T. W.; Parsons, S.; Murugesu, M.; Wernsdorfer, W.; Christou, G.; Brechin, E. K. *Angew. Chem., Int. Ed.* **2005**, *44*, 6540−6543; Mn_{84}, (n) Tasiopoulos, A. J.; Vinslava, A.; Wernsdorfer, W.; Abboud, K. A.; Christou, G. *Angew. Chem., Int. Ed.* **2004**, *43*, 2117−2121.

(10) G. M. Sheldrick, *SADABS 2.05*, University Göttingen: Göttingen, Germany.

(11) *SHELXTL 6.10*; Bruker Analytical Instrumentation: Madison, WI, 2000.

Table 1. Crystallographic Data and Structural Refinements for **1** and **2**

compound	**1**	**2**
molecular formula	$C_{197.5}H_{227}Mn_{30}O_{120}$	$C_{92.5}H_{178}Mn_{15}O_{58}$
fw	6168.98	3042.45
T (K)	120(2)	100(2)
cryst color and form	black plate	black prism
cryst syst	triclinic	trigonal
space group	$P\bar{1}$ (no. 2)	$P\bar{3}$ (no. 147)
a (Å)	21.215(2)	23.614(1)
b (Å)	22.494(2)	23.614(1)
c (Å)	29.539(3)	13.492(2)
α (deg)	91.468(2)	90
β (deg)	97.911(2)	90
γ (deg)	109.603(1)	120
V (Å^3)	13 114(2)	6515.3(9)
Z	2	2
D_{calcd} (g cm^{-3})	1.562	1.551
μ (mm^{-1})	1.478	1.485
θ range (deg)	1.15 to 25.00	1.30 to 25.00
reflns (collected/unique)	93 593/45 694	23 515/7610
completeness (%)	98.9	99.2
params	2871	508
GOF	1.012	1.031
R1 [$I \geq 2\sigma(I)$][a,b]	0.0783	0.0589
wR2 (all data)[a,b]	0.2580	0.1720
Residues (e Å^{-3})	1.327 and −0.795	0.792 and −0.456

[a] $R1 = \Sigma||F_o| - |F_c||/\Sigma|F_o|$. [b] $wR2 = [\Sigma w(F_o^2 - F_c^2)^2/\Sigma w(F_o^2)^2]^{1/2}$.

Scheme 1 Ligand Substitution Reaction

$$[Mn^{III}_9Mn^{IV}_6(O_2CPh)_{12}(\mu_3\text{-}O)_{13}(\mu\text{-}O)_4(\mu\text{-}OMe)_5(MeOH)_4(H_2O)_5] + 12ChCO_2H + H_2O \longrightarrow \underset{\mathbf{1}}{} [Mn^{III}_9Mn^{IV}_6(O_2CCh)_{12}(\mu_3\text{-}O)_{13}(\mu\text{-}O)_4(\mu\text{-}OMe)_5(MeOH)_3(H_2O)_6] + 12PhCO_2H + MeOH \quad (1)$$
$$\underset{\mathbf{2}}{}$$

and structure solution details are listed in Table 1. Selected bond distances and angles are listed in Tables S1 and S2.

Magnetic Study. Magnetic susceptibility measurements of **1** and **2** were performed with a Quantum Design MPMS-XL7 SQUID. Polycrystalline samples of **1** and **2** were embedded in vaseline to prevent torquing. All of the ac susceptibility data were collected at zero dc field and 5 Oe ac amplitude. Data were corrected for the diamagnetic contribution calculated from Pascal constants.

3. Results and Discussion

Synthesis. The unprecedented Mn_{15} core was synthesized via a conventional manganese redox reaction (MnO_4^- oxidizing Mn^{2+}) in a benzoic acid−methanol solution. The formation of **1** and **2** rather than other previously reported manganese species may be attributed to the long period of vigorous stirring, which also produces a lot of unknown black precipitate. Therefore, the yield of **1** is not so high (30−40%). To eliminate the intermolecular $\pi-\pi$ stacking interactions, which we considered as the biggest hindrance in observing the slow-magnetic relaxation behavior in **1** (below), we attempted to replace the benzoate with an analogous σ-bonded and stronger cyclohexanecarboxylate that can efficiently separate the intercluster magnetic interactions.[12] Fortunately, the replacement led to the formation of **2** (Scheme 1) in high yield, which presents the first site-specific ligand substitution taking place on the manganese cluster with a nuclearity greater than 12, although such substitution has long been succeeded in the Mn_{12} clusters.[5]

Crystal Structures. Single-crystal structures of **1** and **2** feature similar disklike Mn_{15} clusters (Figure 1), formulated as $[Mn^{III}_9Mn^{IV}_6(O_2CR_1)_{12}(\mu_3\text{-}O)_{13}(\mu\text{-}O)_4(\mu\text{-}OMe)_5(HOR_2)_9]$ (R_1 = phenyl or cyclohexane, R_2 = H or Me). Each Mn_{15} core contains six coplanar Mn^{IV} ions in the bottom, nine noncoplanar Mn^{III} ions at the edges, 13 μ_3-O^{2-} ions as the bridges between Mn^{III} and Mn^{IV} ions, and 12 carboxylates on the outer shell. In addition, the Mn^{III} and Mn^{IV} ions are also bridged by disordered μ-O^{2-} and μ-OMe groups (Scheme 2a). The disordered μ-O^{2-} and μ-OMe groups have a total ratio of 5:4, according to the charge−balance requirement and elemental analysis. This conclusion is also supported by Bond Valence Sum (BVS) calculations[13] (Table S3) on these disordered oxygen positions, which give values in range of 1.32(2) to 1.54(1), significantly larger than 1.0 for a normal monovalence μ-OMe group, yet smaller than 2.0 for a normal divalent μ-O^{2-} group. A similar situation was observed in some other manganese-based SMMs.[9d,h] The overall structure of the Mn_{15} core has significant similarity to that of Mn_{12}.[12c] Both the Mn_{12} and Mn_{15} cores comprise a nonplanar Mn^{III}_x ring around a central Mn^{IV}_y unit, except that the central Mn^{IV} ions of Mn_{15} are coplanar and quite below the ring of Mn^{III}_x, whereas the central Mn^{IV} ions of Mn_{12} are in a cube and almost coplanar with the ring Mn^{III}_x units. The members of this family now include Mn_{12} ($x = 8$, $y = 4$), Mn_{15} ($x = 9$, $y = 6$), Mn_{16} ($x = 10$, $y = 6$),[9c,d] and Mn_{21} ($x = 12$, $y = 9$).[9g]

Nevertheless, the difference between the Mn_{15} cores in **1** and **2** is also evident from the structural parameters. The cluster in **1** contains only C_1 symmetry, although it bears a pseudo-C_3 axis (defined as perpendicular to the plane comprising the six Mn^{IV} ions) passing through the central μ_3-O^{2-} ion. In contrast, the cluster in **2** contains a crystal-

(12) (a) Kramer, L. S.; Clauss, A. W.; Francesconi, L. C.; Corbin, D. R.; Hendrickson, D. N.; Stucky, G. D. *Inorg. Chem.* **1981**, *20*, 2070−2077. (b) Zheng, Y.-Z.; Tong, M.-L.; Zhang, W.-X.; Chen, X.-M. *Angew. Chem., Int. Ed.* **2006**, *45*, 6310−6314. (c) Zheng, Y.-Z.; Tong, M.-L.; Zhang, W.-X.; Chen, X.-M. *Chem. Commun.* **2006**, 165−167.

(13) Brown, I. D.; Altermatt, D. *Acta Crystallogr., Sect. B* **1985**, *41*, 244−247.

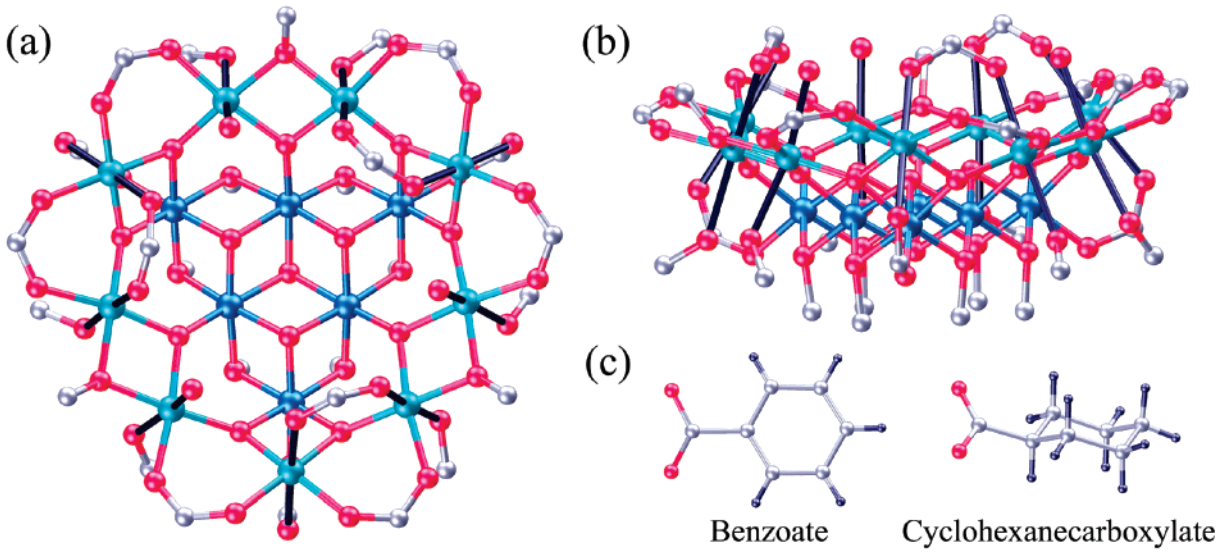

Figure 1. Topview (a) and sideview (b) of the disklike Mn_{15} core, as well as two carboxylate ligands (c). Color codes: Mn^{III}, cyan; Mn^{IV}, blue, O, red; C, gray; and the elongated Jahn−Teller axes of Mn^{III} ions are highlighted in black (the same setting as the following figures).

Scheme 2. Disordered Mode of μ-O^{2-} and μ-OMe^{-} (a); Disordered Mode of Terminal H_2O and MeOH (b) in Both **1** and **2**; and Disordered Mode of μ-O_2CPh^{-} with Adjacent Terminal H_2O Ligands in **1** Only (c)

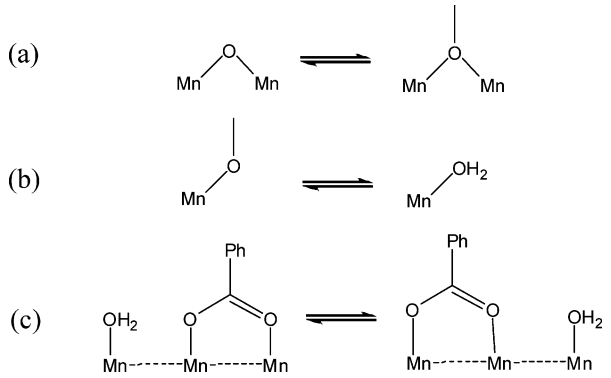

lographic C_3 axis passing through the central μ_3-O^{2-} ion. Moreover, the total ratio of the disordered terminal MeOH and H_2O ligands (Scheme 2b) on the Mn_{15} cores are also different, being 4:5 and 3:6 in **1** and **2**, respectively, and the distribution of these ligands is significantly inhomogeneous in **1** (i.e., some positions are occupied by only a water ligand or only a methanol ligand), whereas it is homogeneously disordered with a half-to-half occupancy in **2**. These particular arrangements are considered as the main reason leading to the loss of a true C_3 symmetry for the Mn_{15} core in **1**. Although these differences are inconspicuous, they have a significant influence on the local geometry of the Mn^{III} ions. As shown by the bond distances and angles (Tables S1 and S2), each Mn^{IV} ion in **1** and **2** has a similar, slightly distorted octahedral geometry with a mean Mn−O bond length of 1.889(2) and 1.890(2) Å for **1** and **2**, respectively. Meanwhile all of the Mn^{III} ions are in elongated octahedra with mean equatorial Mn−O bond lengths of 1.917(6) Å in **1** and 1.914(4) Å in **2** and a mean axial Mn−O bond (Jahn−Teller axes, denoted by JT hereafter) length of 2.225(8) Å in **1**, being slightly shorter than 2.237(5) Å in **2**. Similarly, the mean O−Mn−O angle of the JT axes is 172.2(3)° in **1**, being a bit smaller than 174.2(2)° in **2**. These comparisons show that the elongations of the octahedra in **2** are more significant than those in **1**. In fact, the elongated JT axes are usually referred to as the weakest bonds among the coordination bonds of a metal center.[14] As shown in Figure 1, the JT bonds in Mn_{15} are associated with carboxylate, methanol, and water oxygen atoms. It should be noted that the JT bonds in the inner-disk side comprise six oxygen atoms from three carboxylate ends and three oxygen atoms from three aqua ligands, and these oxygen positions are highly disordered in one of two independent Mn_{15} molecules in **1** (Scheme 2c). As such, the weak Mn−O(carboxy) bonds provide the chance for substitution by a stronger donor $ChCO_2^{-}$ ligand, and consequently, this disorder disappears in **2**. Moreover, all of the mean closest intramolecular Mn···Mn distances in **2** are slightly shorter than those in **1** (i.e., Mn^{IV}···Mn^{IV} 2.836(1) vs 2.842(2) Å, Mn^{III}···Mn^{III} 3.214(1) vs 3.225(2) Å and Mn^{III}···Mn^{IV} 3.290(1) vs 3.293(2) Å for **2** and **1**, respectively), suggesting that the Mn_{15} core in **2** is more compact than that in **1**.

In contrast to the small geometric differences in the Mn_{15} cores, the crystal packing differences in **1** and **2** are more pronounced. The orientations (Figures 2a and S1) of the disklike Mn_{15} cores in **1** are somewhat intricate due to the low crystallographic symmetry. Each pair of the Mn_{15} molecules in **1** is only inversely related, having significant intercluster $\pi-\pi$ stacking interactions between the phenyl rings with the short distances of 3.38 Å for face-to-face and

(14) For large D_m values of manganese-based SMMs, see Mn_2, (a) Miyasaka, H.; Clérac, R.; Wernsdorfer, W.; Lecren, L.; Bonhomme, C.; Sugiura, K.-i. *Angew. Chem., Int. Ed.* **2004**, *43*, 2801−2805; Mn_6, (b) Milios, C. J.; Raptopoulou, C. P.; Terzis, A.; Lloret, F.; Vicente, R.; Perlepes, S. P.; Escuer, A. *Angew. Chem., Int. Ed.* **2004**, *43*, 210−212; Mn_{12}, (c) Sessoli, R.; Gatteschi, D.; Caneschi, A.; Novak, M. A. *Nature* **1993**, *365*, 141−143; Mn_{30}, (d) Soler, M.; Rumberger, E.; Folting, K.; Hendrickson, D. N.; Christou, G. *Polyhedron* **2001**, *20*, 1365−1369. For large D_m values of non-manganese SMMs, see (e) Wang, C.-F.; Zuo, J.-L.; Bartlett, B. M.; Song, Y.; Long, J. R.; You, X.-Z. *J. Am. Chem. Soc.* **2006**, *128*, 7162−7163. (f) Li, D.; Clérac, R.; Parkin, S.; Wang, G.; Yee, G. T.; Holmes, S. M. *Inorg. Chem.* **2006**, *45*, 5251−5253.

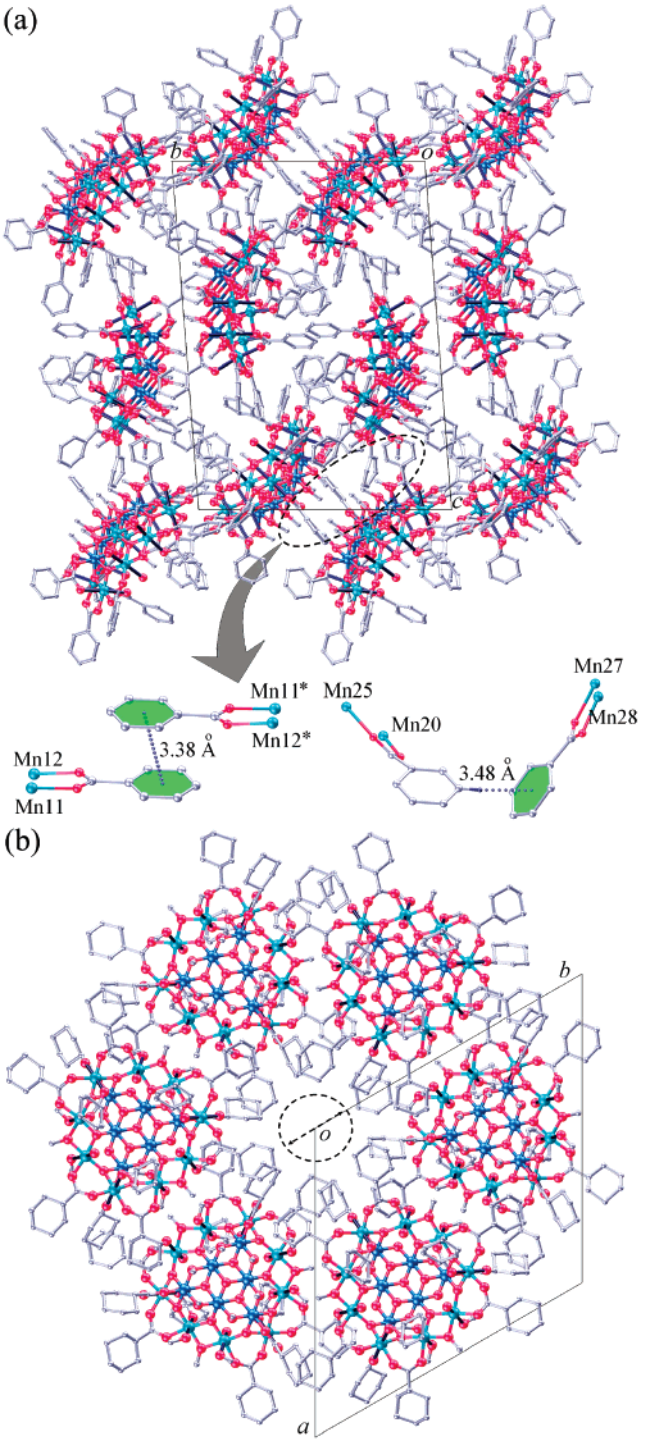

Figure 2. Perspective views of the crystal packings along the *a* axis and $\pi-\pi$ stacking interactions in **1** (a) and along the *c* axis in **2** (b).

3.48 Å for edge-to-face $\pi-\pi$ stacking.[15] The shortest intercluster Mn···Mn distance is 7.380 Å in **1**. As shown in Figures 2b and S2, the disklike Mn_{15} cores in **2** are all orderly arranged around the *c* axis with the disk bottom pointing alternately up and down in relation to the I_3 symmetry, featuring no strong intercluster interaction other than van der Waals forces. The shortest intermolecular Mn···Mn distance is 7.579 Å in **2**, being slightly longer than that in **1**.

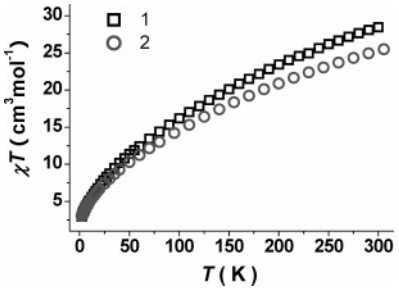

Figure 3. Plots of χT versus *T* at an applied field of 1000 Oe for **1** and **2**.

Interestingly, the packing of the Mn_{15} molecules in **2** leaves a channel with an effect diameter of ca. 3.77 Å along the *c* axis to accommodate the solvent molecules that cannot be totally determined by X-ray single-crystal diffraction.

Magnetic Properties. The structural effects on the magnetic properties of **1** and **2** are very interesting. The dc susceptibility data under an applied field of 1000 Oe (Figure 3) show that the χT values at 300 K are 28.46 and 25.49 $cm^3\ mol^{-1}\ K$ per Mn_{15} molecule for **1** and **2**, respectively. Both of the values are much smaller than the expected spin-only value of 38.21 $cm^3\ mol^{-1}\ K$ for a noninteracting $Mn^{III}_9Mn^{IV}_6$ unit, indicating a dominant antiferromagnetic coupling between the metal centers. This phenomenon is very common in some antiferromagnetic manganese clusters.[9d,e,o] The smaller χT value for **2** is probably due to the more compact arrangement of the Mn_{15} core that leads to stronger antiferromagnetic interactions. Upon cooling, the χT values gradually decrease to 2.97 and 3.03 $cm^3\ mol^{-1}\ K$ at 2 K for **1** and **2**, respectively. These values correspond very well to $S_T = 2$ and $g = 2$. Moreover, the χT values from 10 to 2 K are virtually identical to the $\chi' T$ values from the temperature-dependent in-phase (χ') alternating current (ac) magnetic susceptibility (Figure S3), confirming that both **1** and **2** have the same ground spin state $S_T = 2$. This method is regarded as the most reliable way to determine the ground states of molecules with low-lying excited states even at the low temperature employed.[9d,e,o] $S_T = 2$ corresponds very well to a spin-coupling scheme in which all of the manganese centers are antiferromagnetically coupled, leading to only one Mn^{III} spin retained for the odd number of the total Mn^{III} spins (for details, see Scheme S1).

For such a small S_T, we can hardly expect the presence of SMMs behavior for **1** or **2**. This is the exactly case for **1**. However, a clearly frequency-dependent out-of-phase signal is observed for **2** (Figure 4). This surprising behavior is a very positive signal for the SMMs behavior although it does not mean all, because spin-glass or random-domain magnets can also lead to such signals.[16] To further investigate this behavior, isothermal frequency-dependent ac susceptibility data were collected to evaluate the effective energy barrier for **2** (Figure 5). The data were fitted by a generalized Debye model (for details, see Eqs S1 and S2, and Figure S4). The obtained τ values from χ'' are further used and fitted by the Arrhenius law [$\tau = \tau_0 \exp(U_{eff}/k_BT)$], giving $U_{eff} = 8.9(1)$ K

(15) Steed, J. W.; Atwood, J. L. *Supramolecular Chemistry*; John Wily & Sons: Chichester, U.K., 2000.

(16) Mydosh, J. A. *Spin Glasses: An Experimental Introduction*; Taylor & Francis: London, U.K. 1993.

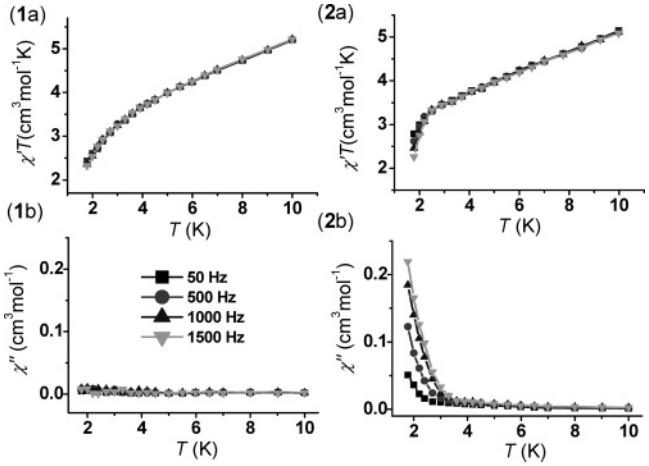

Figure 4. Temperature dependence of the in-phase (**1**a and **2**a for **1** and **2**, respectively) and out-of-phase (**1**b and **2**b for **1** and **2**, respectively) ac susceptibility at the indicated frequencies.

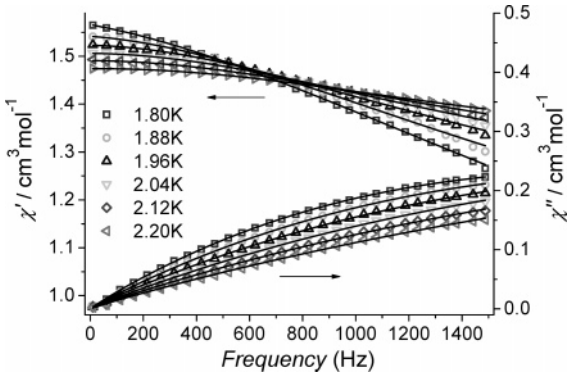

Figure 5. Isothermal frequency-dependent ac susceptibility plots for **2**. The solid lines are least-squares fits of the data to a distribution of relaxation processes with a generated Debye model.

and $\tau_0 = 5.25 \times 10^{-7}$ s. Magnetization data were also collected in a dc magnetic field and in temperature ranges of 0.1−7.0 T and 1.8−4.0 K, respectively, and were fitted by the program ANISOFIT 2.0.[17] However, attempts to fit the data above 3 T were unsuccessful, which suggests that possible low-lying excited states are still populated. This presumption is consistent with the isothermal field-dependent magnetization at 1.8 K (Figure 6), in which the maximum value of **1** and **2** reaches $5.32\mu_B$ and $4.95\mu_B$ at 7 T, respectively. These values are significantly larger than $4\mu_B$, as expected for the $S_T = 2$ (assuming $g = 2$) ground states, unambiguously indicating the existence of the low-lying excited states even at the operating limit of our SQUID. However, it does not affect **2** to behave as an SMM. The best fits were carried by using the low-field data (0.1−2.0 T), which is also regarded as the reliable way in determining the ground states of molecules with low-lying excited states.[9d,e,o] This alteration gives very good fitting results (Figure 7) with $g_1 = 2.00$, $D_{m1} = -0.89$ cm^{-1}, and $E_{m1} = 9.5 \times 10^{-2}$ cm^{-1} for **1**, and $g_2 = 1.99$, $D_{m2} = -1.58$ cm^{-1}, and $E_{m2} = 3.1 \times 10^{-4}$ cm^{-1} for **2**. Other

(17) This program assumes that only the ground states are populated, including D_m, E_m, g, and Zeeman interactions and incorporating a full powder average; for details see Shores, M. P.; Sokol, J. J.; Long, J. R. *J. Am. Chem. Soc.* **2002**, *124*, 2279−2292.

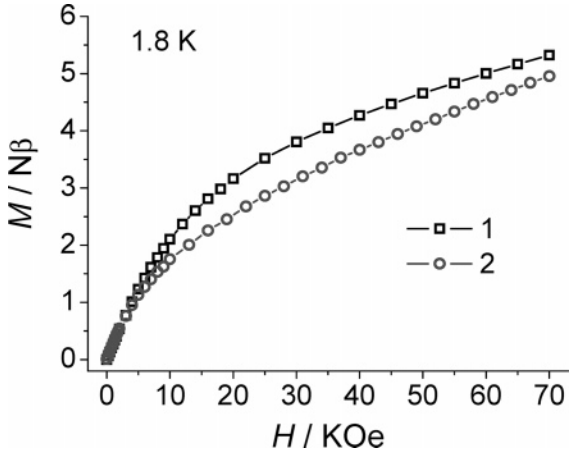

Figure 6. Plots of M versus H/T for **1** (a) and **2** (b) at the indicated applied fields. The solid lines are the best fits of the data.

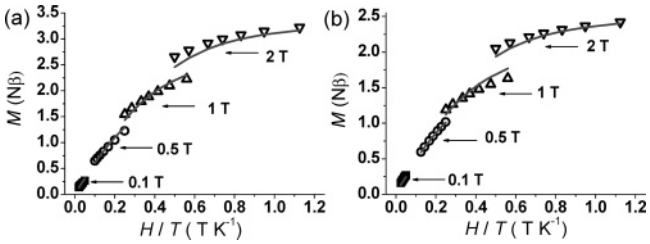

Figure 7. Plots of M versus H of **1** and **2** at 1.8 K.

attempts of fitting by using higher values of S_T are inferior. These fitting results are very informative. D_{m2} corresponds to an energy barrier ($U = D_m S_T^2$ for integer spins) of 9.03 K, an almost 2-fold increase in comparison to that of **1** (5.09 K). This large difference in the energy barrier is responsible for the different ac magnetic behaviors. The absence of χ'' above 1.8 K in **1** is clearly due to the small energy barrier that can not, on one hand, block the spin reversal caused by k_BT, and on the other hand, stand the "wastage" of the QTM effect as indicated by a relative larger E_m value.[2,3] In contrast, the U_{eff} of **2** is almost equal to U, implying that the QTM effect in **2** should be very ineffective. This observation is consistent with the strictly C_3 symmetry of **2**,[2,3] which is also confirmed by the very large D_m/E_m ratio.

Discussion

The obtained D_m values for **1** and **2** are both large in the manganese-based SMMs, suggesting a large axial anisotropy in the two compounds. Accurate evaluation of D_m requires single-crystal high-frequency EPR (HFEPR) studies,[2] which, in any case, are also complicated by low-lying excited states.[2c] In fact, the large D_{m2} value is consistent with the alignment of 9 JT axes of the Mn^{III} ions, which all point to the central C_3 axis with an average angle (denoted as α, it is an approximate gauge of the angle between the local JT axes and the principal axis of the susceptibility tensor of the molecule[2,4a] (for details, see Table 2) of 27.5(1)° in **2**, a bit smaller than 28.1(1)° (refer to the pseudo-C_3 axis) in **1**. In other words, the JT axes in **2** are more parallel to the principal axis of the susceptibility tensor. Such arrangement of the JT axes easily leads to a large negative D_m, which has been

Table 2. Angle (α) between the JT Direction and the Pseudo- or True-C_3 Symmetric Axes in **1** and **2**

1			
atom	α (deg)	atom	α (deg)
Mn7	25.54	Mn22	32.04
Mn8	33.44	Mn23	24.58
Mn9	25.28	Mn24	21.76
Mn10	20.55	Mn25	32.98
Mn11	32.95	Mn26	28.64
Mn12	29.54	Mn27	24.17
Mn13	27.58	Mn28	31.79
Mn14	34.47	Mn29	29.00
Mn15	21.26	Mn30	29.19
2			
Mn3	37.40	Mn5	24.06
Mn4	20.90		

confirmed by the reported Mn_2, Mn_6, Mn_{12}, Mn_{21}, and Mn_{30} SMMs with roughly parallel Mn^{III} JT axes.[12,9g] Moreover, the average D_i in **2** is probably larger than that in **1** because the Mn^{III} octahedra in **2** are more elongated than those in **1** and, consequently, leads to a larger D_i.[18] The two reasons mentioned above are crucial to the enhancement of the magnetic anisotropy of the Mn_{15} core in **2**, because the vectorial projection of single-ion Mn^{III} anisotropies (octahedral Mn^{IV} are fairly isotropic ions) onto the molecular anisotropy axis determines the main magnitude of the molecular D_m value.[19] In addition to the above reasons, another source of anisotropy that would affect the whole molecular anisotropy is inter-single-ion dipole−dipole interaction (D_{ij}, for details, see Eq S3), which has two different origins, namely through space and through bonding. The former would be very positive for **2** to reinforce the axial anisotropy because all of the Mn_{15} molecules are arranged in parallel fashion, whereas the opposite result in **1** would be predicted because of the unorderly orientations of the Mn_{15} molecule.[20] The latter would also be better for **2** because of the more compact arrangement of the Mn_{15} core, which leads to stronger magnetic exchange interactions.[19] Therefore, a larger axial magnetic anisotropy would be expected in **2** according the above analysis.

(18) (a) Boča, R. *Coord. Chem. Rev.* **2004**, *248*, 757−815. (b) Boča, R. *Struct. Bonding* **2006**, *127*, 1−264.

(19) If one omits the contribution from the dipole−dipole interaction D_{ij}, then $D_m \propto d_i D_i \cos^2(\alpha)$, where d_i is the coefficient related to the coupling scheme one chooses. From this correlation, one can see that the contribution of the larger D_m value in **2** is mainly related to three components, namely d_i, D_i, and α; for details see Scheme S1, Eq S3, refs 2a, 2c, and 4a.

4. Conclusion

This work demonstrates the synthesis of a new disklike Mn_{15} species, and more significantly, the effect of site-specific ligand substitution on the ground-state anisotropy of two Mn_{15}-carboxylate clusters, which may provide a practical way to control the molecular symmetry, tunneling mechanisms, and intermolecular interactions.

Acknowledgment. This work was supported by the NSFC (grants 20531070 and 20525102) and Science and Technology Department of Guangdong Province (grant 04205405).

Supporting Information Available: Crystal data (CIF file, additional structural data and plots) and additional magnetic data. This material is available free of charge via the Internet at http://pubs.acs.org.

IC7004584

(20) $D_{ij} \propto J/r^3$, where J is the coupling constant and r is the distance between the single ions; for details see Eq S3, refs 2a, 2c, and 4.